Journal of Materials Science: Materials in Electronics (2020) 31:15007–15012
https://doi.org/10.1007/s10854-020-04064-5

Enhanced photocatalytic activity of Ba doped $BiFeO_3$ by turning morphologies and band gap

Yaowen Zhang[1] · Yonghang Yang[1] · Zhichen Dong[3] · Junchen Shen[1] · Qinxin Song[1] · Xingfu Wang[1] · Weiwei Mao[1,2] · Yong Pu[1] · Xing'ao Li[1,2,3]

Received: 7 May 2020 / Accepted: 21 July 2020 / Published online: 29 July 2020

Abstract
The application of $BiFeO_3$ (BFO) in the treatment of environmental water pollution is very important. In this paper, Ba-doped bismuth ferrite series nanomaterials were prepared by sol–gel method. The results of X-ray diffraction show the evolution of the crystal structure by doping of Ba, while it can be seen by scanning electron microscopy that the doping reduces the grain size gradually. The band gap gets narrow after doping with Ba, result in high efficiency for the degradation of methyl orange under visible light irradiation. Furthermore, it is found that the ferromagnetism increases with the increase of Ba doping. Therefore, the BFO-based photocatalyst can be obtained by Ba doping with good performance.

1 Introduction

Nowadays, the only fresh water resources we have, is suffering from domestic sewage, industrial waste water and the early rain, water has become a dangerous, always endangering human health. Therefore, convenient and efficient sewage treatment has become one of the world's major issues to be urgently solved. Photocatalytic technology mainly uses to degrade pollutants through reduction or oxidation of ultraviolet or visible light irradiation [1–3]. In this respect, $BiFeO_3$ (BFO), as a new visible light responsive semiconductor photocatalytic material, has gradually demonstrated its advantages in new energy and environmental pollution control [4–6].

Perovskite-type BFO is one of the few multiferroic materials with both ferroelectricity and weak ferromagnetism at room temperature [7, 8]. In addition to the application of magnetoelectric properties, $BiFeO_3$ has a good photocatalytic application prospect due to its narrow band gap (2.2 eV) and high physical stability [5]. BFO synthesized by hydrothermal method can improve the photocatalytic performance by changing the alkaline environment of hydrothermal reaction or adding surfactant to modify the morphology [9–11]. In addition, ion doping is also an effective means to improve the photocatalytic performance. For example, the Gd-doped BFO nanoparticles prepared by sol–gel method not only enhance ferromagnetism, but also obtain good photocatalytic performance [12]. And 1% content of Y doping, can effectively influence the BFO band gap and the specific surface area, thereby enhancing photocatalytic degradation towards methylene blue [13]. Irfan et al. found that the co-doping of La and Se can not only reduce the band gap of BFO, but also effectively reduce the composition of photo-generated electron holes, thus enhancing the photocatalytic activity [14]. In the past studies, it has been found that alkaline soil ion doping can also effectively regulate the performance of BFO, and is cheaper than rare earth ions, which is convenient for promotion and application [15–17]. Therefore, Ba ion was selected to dope into BFO in this project, and the influence of Ba doping on its crystal structure,

✉ Weiwei Mao
maoww@njupt.edu.cn

✉ Yong Pu
puyong@njupt.edu.cn

✉ Xing'ao Li
lxahbmy@126.com

[1] New Energy Technology Engineering Laboratory of Jiangsu Province & School of Science, Nanjing University of Posts and Telecommunications (NJUPT), Nanjing 210023, China

[2] National Laboratory of Solid State Microstructures, Nanjing University, Nanjing 210093, China

[3] Key Laboratory for Organic Electronics and Information Displays & Institute of Advanced Materials (IAM), Jiangsu National Synergetic Innovation Center for Advanced Materials (SICAM), Nanjing University of Posts & Telecommunications, Nanjing 210023, China

morphology, band gap and photocatalytic performance were studied.

2 Experimental

The $Bi_{1-x}Ba_xFeO_3$ ($x = 0$, 0.05, 0.075, 0.10) samples were prepared by sol-gel method. First, raw materials $Bi(NO_3)_3{\cdot}5H_2O$, $Fe(NO_3)_3{\cdot}9H2O$, $Ba(NO_3)_2$ were weighed according to molar ratio. $Fe(NO_3)_3{\cdot}9H_2O$ and $Bi(NO_3)_3{\cdot}5H_2O$ are ultrasonic dissolved in ethylene glycol, and $Ba(NO_3)_2$ was dissolved in deionized water. After the above materials are completely dissolved into a clear solution, the two groups of solutions are mixed, heated and stirred on a magnetic mixer until the gel is formed. The gel was dried for 24 h at 70 °C, then taken out and calcined at 600 °C for 2 h. Finally, the power was cooled naturally at room temperature, and then the required samples were prepared.

We studied the phase purity and crystal structure of the sample powder by X-ray diffraction (XRD), the morphology of the sample was characterized by scanning electron microscope (SEM), the magnetization hysteresis curve was measured by SQUID magnetometer. UV–visible absorption spectra were obtained using a PerkinElmer Lambda 35 spectrophotometer.

The photocatalytic activities were evaluated by degradation of methyl orange aqueous solution under visible light irradiation: Weigh a certain amount of BFO, prepare 100 mL of methyl orange solution with mass concentration of 10 mg/L in a three-necked flask, and add a certain amount. A 500 W Xe lamp was used as the light source, and visible-light irradiation was realized by attaching a 420 nm cutoff filter. After irradiation, the suspension of 3 ml was separated out of the photocatalyst by centrifugation and taken every 30 min. The absorbance amount of methyl orange was measured by using an ultraviolet–visible light spectrophotometer.

3 Results and discussion

The XRD diffraction spectra of all the samples at room temperature are shown in Fig. 1a. All diffraction peaks correspond well to the BFO standard card of R3c space group (JCPDS file no.71-2494) [18, 19]. There is no obvious impurity phase in the XRD pattern. In particular, no obvious second phase such as BaO in the doped BFO, so it can be judged that Ba ion has successfully doped into BFO lattice. Figure 1b shows an enlarged view of the diffraction angle between 31° and 33°, from which the evolution of the diffraction peaks (104) and (110) after doping can be obtained. With the doping of Ba^{2+} ions, the diffraction peaks of (104) and (110) are shifted to lower Angle. This is because the radius of Ba^{2+} is 1.42 Å, which is greater than the radius of Bi^{3+} (the coordination number is 8) [20]. With the increase of Ba^{2+} content, the diffraction peaks of (104) and (110) remained basically the same, but the splitting of the two peaks weakens and the merging trend is more obvious. This shows that the higher the doping concentration of Ba ion, the greater the structural distortion.

The surface morphological characteristics of all the samples can be observed by SEM, as shown in Figure. The morphology of pure BFO ($x = 0$) is irregular and block-shaped, and the grain size is very uneven, ranging from 100 to 300 nm. Figure 2b shows the SEM of $x = 0.05$. It can be seen that the grain size decreases slightly after Ba doping, which

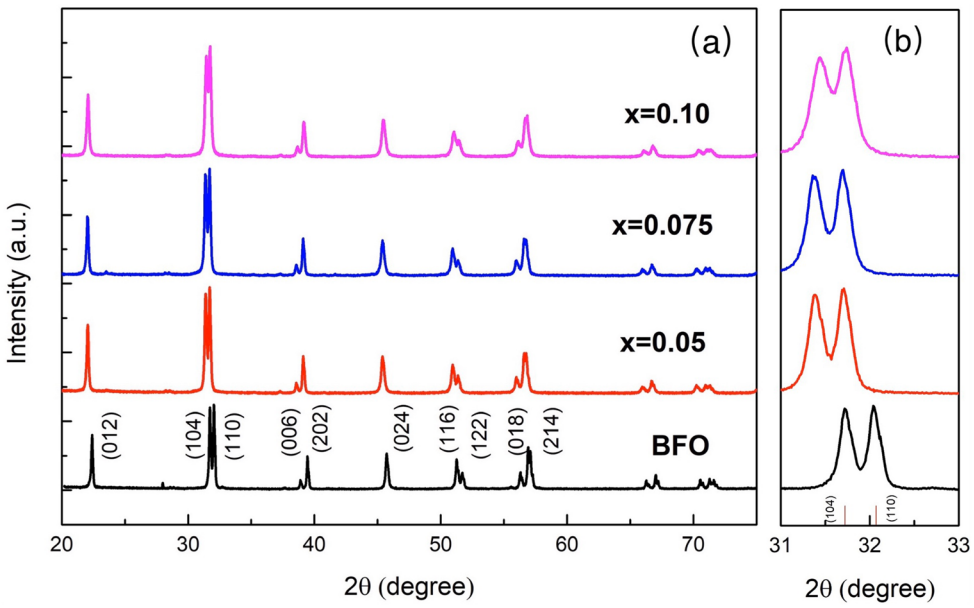

Fig. 1 **a** X-ray diffraction patterns of all the samples measured at room temperature. **b** Enlarged view of the diffraction peaks (104) and (110)

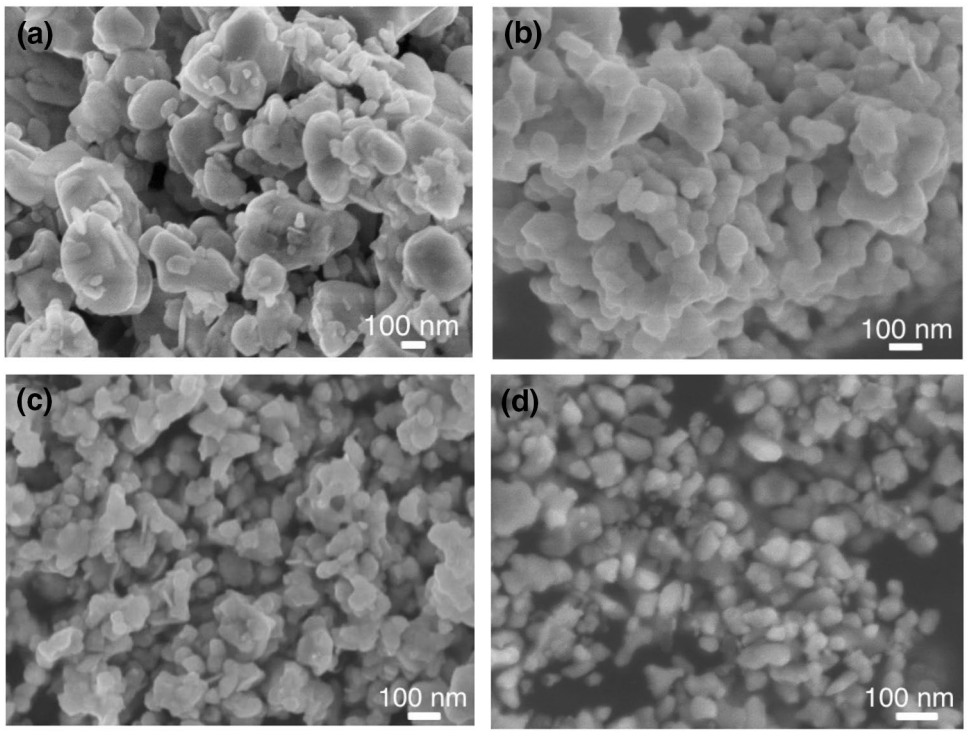

Fig. 2 SEM images for **a** $x=0.00$, **b** $x=0.05$, **c** $x=0.075$, **d** $x=0.10$ samples

is roughly 100 nm to 200 nm. To increase the doping content of Ba, further reducing grain size can be seen in Fig. 2c, d. The grain size of $x=0.075$ sample is about 50 nm–100 nm, and the grain size of $x=0.10$ is about 30 nm–100 nm. It could be that Ba doping has inhibitory effect on the growth of grain [21]. The lattice constant of added Ba is matched with the lattice constant of the substance in the stock solution phase, which becomes the core of heterogeneous nucleation during solidification. Doping Ba acts as an impurity during liquid phase crystallization, and becomes the core of a large number of heterogeneous nucleation, greatly improving the nucleation rate, which results in grain size reduction. Although the grain size decreases significantly after doping, the distribution of grain size in the samples is irregular with an apparent agglomeration.

BFO is a semiconductor whose optical absorption properties are related to the electronic structure and band gap. We characterized the UV–visible diffuse reflectance spectroscopy of the samples doped with $x=0.05$, 0.075 and 0.1, as shown in Fig. 3a. The measured wavelength range is 50–950 nm. As can be seen from the Fig. 3a), there is absorption in the range of about 250–600 nm, which indicates that both ultraviolet region and visible region have response.

The optical band gap can be calculated by Tauc diagram method. Absorption coefficient is related to E_g in this method, where the calculation formula is: $(\alpha h\nu)^2 = A(h\nu - E_g)$, one of the alpha for light absorption coefficient, h is Planck's constant, ν is the reciprocal of wavelength, $h\nu$ to allow transition photon energy directly, A is constant. Let's plot $h\nu$ as the x-coordinate and $(\alpha h\nu)^2$ as the y-coordinate, as shown in Fig. 3b–d. The value of E_g is determined by the intersection of the linear extension of the linear part of the curve with the abscissa. It can be seen from the figure that the corresponding band gap when the doping amount x is 0.05, 0.075 and 0.1 is 1.251 eV, 1.188 eV and 1.122 eV, respectively. The band gap of pure is about 2.2 eV–2.8 eV [22–24]. After doping, the band gap is obviously narrowed, and the corresponding band gap value gradually decreases with the increase of doping content. For BFO samples doped with Ba in our experiment, the unit cell volume increase with the decrease of Ba content, which leads to the local straightening of Fe–O–Fe bond angle on the wall and finally the reduction of band gap. Ba-doped BFO has greater absorption capacity and longer edge wavelength of absorption band than BFO. And Ba doping will cause the formation of impurity energy levels in the forbidden band, resulting in the donor energy level moving above the original valence band or the acceptor energy level moving below the original conduction band, which results in the decrease of E_g of Ba-doped BFO [25–27]. The decrease of band gap leads to the increase of photocatalytic activity.

The photocatalytic performance of BFO doped with Ba was evaluated by the degradation efficiency of methyl orange at room temperature. It can be seen from the Fig. 4 that under the illumination condition without catalyst, methyl orange hardly degrades after 150 min, while the degradation rate is only 10% after adding pure BFO.

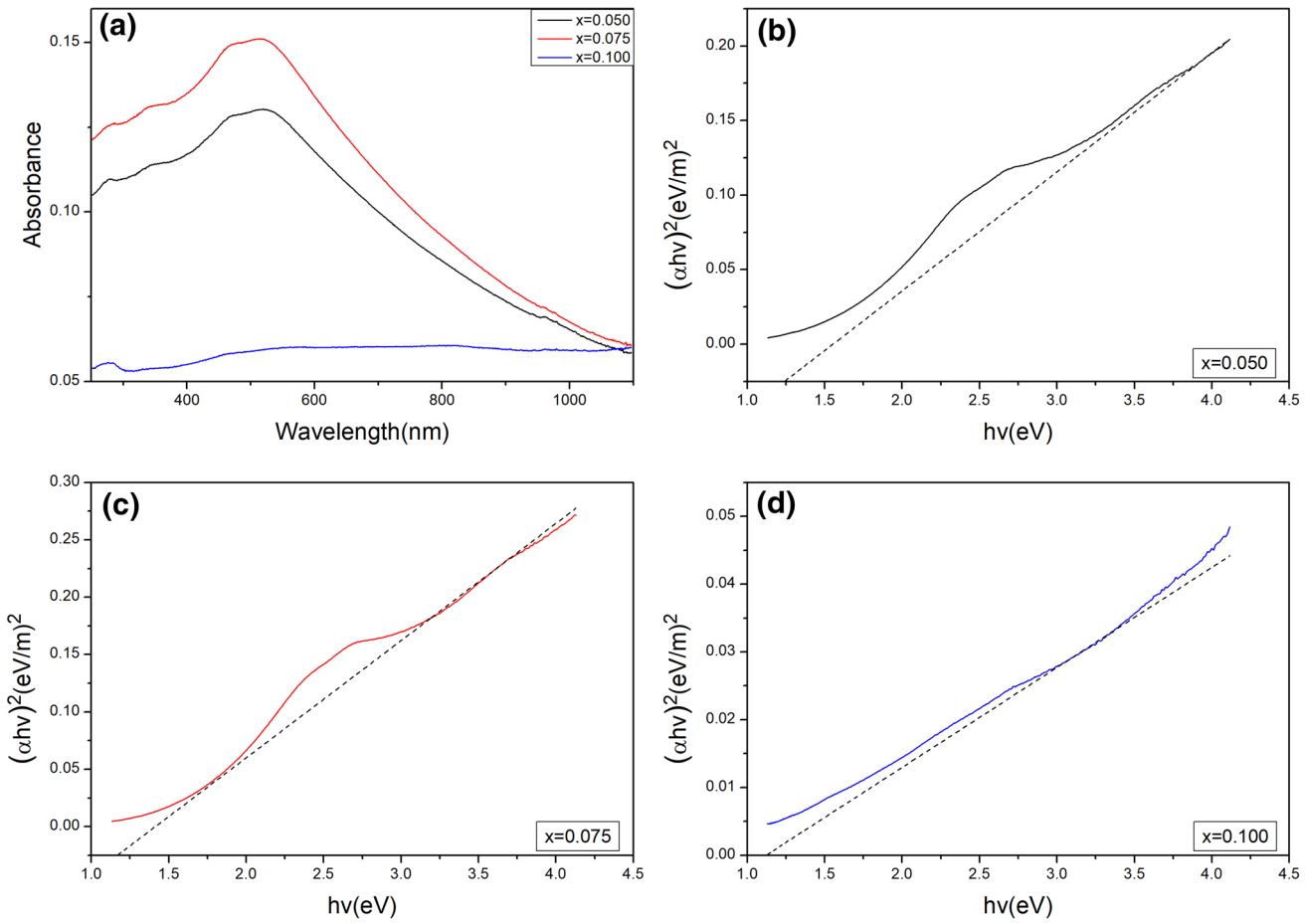

Fig. 3 **a** UV–visible absorption spectra of Ba doped BFO. Tauc's plots to determine the band gap of **b** $x=0.050$, **c** $x=0.075$, **d** $x=0.100$

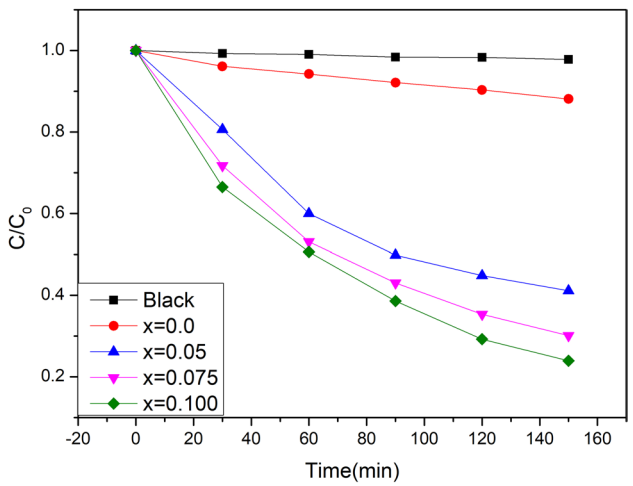

Fig. 4 Photocatalytic activity of all the catalysts for the degradation of methyl orange under visible light irradiation solution at room

After doping Ba ions, the degradation rate of samples was significantly enhanced, and the degradation rate of samples increased gradually with the increase of doped Ba. Combined with the SEM characterization analysis, it is believed that the doping of Ba reduces the geometrical size of the grain and uniformly increases the contact area between the catalyst and methyl orange, which makes the charge transfer more likely, and thus enhances the catalytic efficiency. In addition, combined with the UV–visible absorption spectrum analysis, the band gap of the samples decreases significantly after the doping of Ba ion, which enhanced the light absorption of the catalyst and thus improved the catalytic efficiency.

In order to study the stability of the catalyst, the BFO-based photocatalyst with the best photocatalytic performance of 10% Ba doped BFO was selected for the photocatalytic cycle test, as shown in Fig. 5. The experimental results show that the photocatalytic activity of $x=0.10$ power hardly reduces the photodegradation of methyl orange solution after the second recovery. Even after four cycles, the catalytic efficiency was not significantly reduced, and the degradation rate was still 75%, which indicated that the sample had good stability.

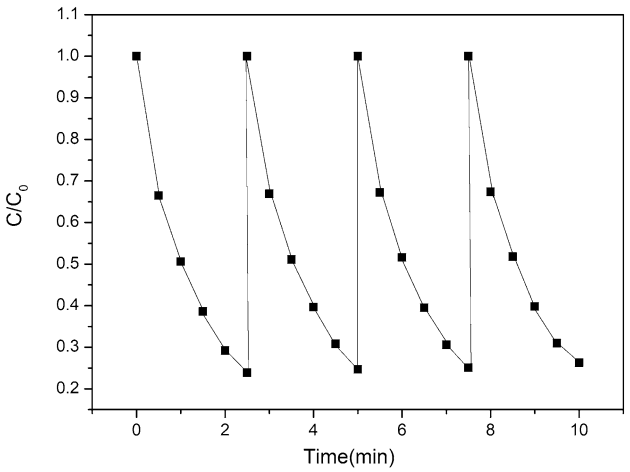

Fig. 5 Cycling runs using $x=0.10$ sample for photocatalytic degradation of methyl orange under visible light irradiation

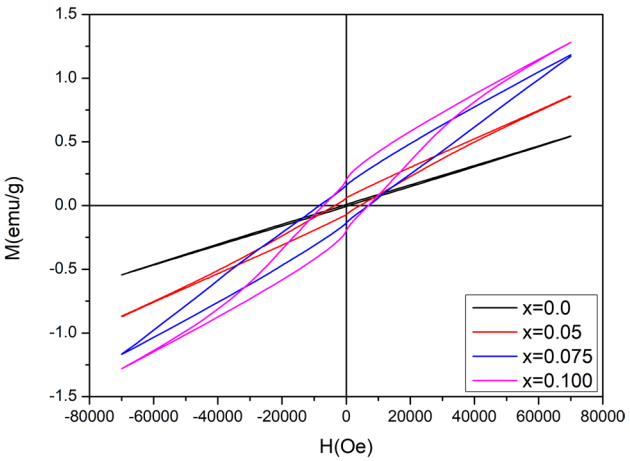

Fig. 6 Magnetization hysteresis (*M–H*) loops of all the samples measured at room temperature

Figure 6shows the magnetized hysteresis loops (*M–H*) with a magnetic field of 70 kOe applied to all samples at room temperature. The pure BFO is antiferromagnetic, which enables the sample to exhibit an almost linear *M–H* loop at a maximum applied magnetic field of 70 kOe with a maximum magnetization (Ms) of 0.506emu/g. As the doping content of Ba increases, the hysteresis loops gradually widen, and the magnetization intensity of Ms and remanent magnetism (Mr) is obviously improved. Therefore, the doping of Ba can significantly improve the ferromagnetism of BFO. As known, BFO is a G-type antiferromagnetic, which can exhibit very weak magnetic properties due to the interaction. But BFO also has a spatially modulated spiral spin structure, resulting in an overall magnetic moment of zero [28]. It can be seen from the XRD analysis that doping will cause the distortion of crystal structure, thus inhibiting the spin modulated structure of BFO, making the magnetic moment appear in a period and enhancing the magnetism [29–31]. The enhanced magnetism allows Ba doped BFO catalyst to be recycled easily from aqueous solution

4 Summary

In summary, this experiment has studied the effects of Ba doping with different contents in BFO on the optical, magnetic and photocatalytic properties. By analyzing the XRD pattern, SEM morphology and UV-visible spectrum, it can be found the influence of structure and morphology of BFO by Ba doping. Especially the band gap gets narrow, which effectively enhanced the photocatalytic performance of BFO. At the same time, the structure distortion caused by doping can also enhance the ferromagnetism, which is of great significance for the application of BFO in the photocatalysis field.

Acknowledgements We acknowledge the National Natural Science Foundation of China (51602161, U1732126, 51872145, 61874060), the Open Project of National Lab of Solid State Microstructures, Nanjing University (M32051, M30044), the Scientific Research Foundation of Nanjing University of Posts and Telecommunications (NY219115), the Scientific Research Foundation of Nanjing University of Posts and Telecommunications (NY219115), STITP of Nanjing University of Posts and Telecommunications (201910293085Y).

References

1. H. Tong, S. Ouyang, Y. Bi, N. Umezawa, M. Oshikiri, J. Ye, Adv. Mater. **24**, 229 (2012)
2. C.G. Silva, R. Juarez, T. Marino, R. Molinari, H. Garcia, J. Am. Chem. Soc. **133**, 595 (2011)
3. Y. Kuang, Y. Gao, J. Zhang, J. Zhao, S. Luo, D. Zhang, C. Lu, Y. Sun, Environ. Sci. Pollut. (2020). https://doi.org/10.1007/s11356-020-09306-x
4. F. Gao, Y. Yuan, K. Wang, X. Chen, F. Chen, J.M. Liu, Z. Ren, Appl. Phys. Lett. **89**, 102506 (2006)
5. F. Gao, X. Chen, K. Yin, S. Dong, Z. Ren, F. Yuan, T. Yu, Z. Zou, J. Liu, Adv. Mater. **19**, 2889 (2007)
6. Y. Huo, M. Miao, Y. Zhang, J. Zhu, H. Li, ChemComm **47**, 2089 (2011)
7. Y. Tokura, S. Seki, N. Nagaosa, Rep. Prog. Phys. Phys. Soc. **77**, 076501 (2014)
8. J. Wang, J.B. Neaton, H. Zheng, V. Nagarajan, S.B. Ogale, B. Liu, D. Viehland, V. Vaithyanathan, D.G. Schlom, U.V. Waghmare, N.A. Spaldin, K.M. Rabe, M. Wuttig, R. Ramesh, Science **299**, 1719 (2003)
9. Y. Huo, Y. Jin, Y. Zhang, J. Mol. Catal. A **331**, 15 (2010)
10. Q. Duan, F. Kong, X. Han, Y. Jiang, T. Liu, Y. Chang, L. Zhou, G. Qin, X. Zhang, Mater. Res. Bull. **112**, 104 (2019)
11. X. Wang, W. Mao, Q. Zhang, Q. Wang, Y. Zhu, J. Zhang, T. Yang, J. Yang, X. Li, W. Huang, J. Alloys Compd. **677**, 288 (2016)
12. R. Guo, L. Fang, W. Dong, F. Zheng, M. Shen, J. Phys. Chem. C **114**, 21390 (2010)

13. N.S. Abdul Satar, R. Adnan, H.L. Lee, S.R. Hall, T. Kobayashi, M.H. Mohamad, N.H. Kassim, Mohd, Kaus, Ceram. Int. **45**, 15964 (2019)
14. S. Irfan, L. Li, A.S. Saleemi, C.-W. Nan, J. Mater. Chem. A **5**, 11143 (2017)
15. H. Chang, F. Yuan, K. Tu, Y. Lo, S. Tu, C. Wang, A. Yang, C. Tu, S. Jen, W. Chang, Jpn. J. Appl. Phys. **117**, 17C734 (2015)
16. C. Yang, J.S. Jiang, F.Z. Qian, D.M. Jiang, C.M. Wang, W.G. Zhang, J. Alloys Compd. **507**, 29 (2010)
17. B. Wang, S. Wang, L. Gong, Z. Zhou, Ceram. Int. **38**, 6643 (2012)
18. D.P. Dutta, O. Jayakumar, A. Tyagi, K. Girija, C. Pillai, G. Sharma, Nanoscale Horiz. **12**, 149 (2010)
19. W. Mao, Q. Yao, Y. Fan, Y. Wang, X. Wang, Y. Pu, X.a. Li, J. Alloys Compd. **784**, 117 (2019)
20. V.A. Khomchenko, V.V. Shvartsman, P. Borisov, W. Kleemann, D.A. Kiselev, I. Bdikin, J.M. Vieira, A.L. Kholkin, J. Phys. D **42**, 045418 (2009)
21. C. Nayek, A. Tamilselvan, C. Thirmal, P. Murugavel, S. Balakumar, J. Appl. Phys. **115**, 073902 (2014)
22. T. Choi, S. Lee, Y.J. Choi, V. Kiryukhin, S. Cheong, Science **324**, 63 (2009)
23. S.R. Basu, L.W. Martin, Y. Chu, M. Gajek, R. Ramesh, R.C. Rai, X. Xu, J.L. Musfeldt, Appl. Phys. Lett. **92**, 091905 (2008)
24. X. Xu, T.V. Brinzari, S.J. Lee, Y. Chu, L.W. Martin, A. Kumar, S. Mcgill, R.C. Rai, R. Ramesh, V. Gopalan, Phys. Rev. B **79**, 134425 (2009)
25. R. Pengrong, F. Huiqing, G. Dong, J. Alloys Compd. **615**, 916 (2014)
26. T. Li, H. Fan, C. Long, G. Dong, S. Sun, J. Alloys Compd. **609**, 60 (2014)
27. G. Dong, H. Fan, H. Tian, J. Fang, Q. Li, RSC Adv. **5**, 29618 (2015)
28. I. Sosnowska, T.P. Neumaier, E. Steichele, J. Phys. C **15**, 4835 (1982)
29. S. Chauhan, M. Kumar, H. Pandey, S. Chhoker, S.C. Katyal, J. Alloys Compd. **811**, 151965 (2019)
30. S. Chauhan, M. Kumar, S. Chhoker, S.C. Katyal, M. Singh, RSC Adv. **6**, 43080 (2016)
31. T. Wang, X.L. Wang, S.H. Song, Q. Ma, Ceram. Int., 15228 (2020)